Isothermal Behavior of the Soret Effect in Nonionic Microemulsions: Size Variation by Using Different n-Alkanes

ARTICLE *in* THE JOURNAL OF PHYSICAL CHEMISTRY B · FEBRUARY 2014

Impact Factor: 3.3 · DOI: 10.1021/jp412126n · Source: PubMed

6 AUTHORS, INCLUDING:

Philipp Naumann
Forschungszentrum Jülich
3 PUBLICATIONS **9** CITATIONS
SEE PROFILE

H. Frielinghaus
Forschungszentrum Jülich
137 PUBLICATIONS **1,420** CITATIONS
SEE PROFILE

Simone Wiegand
Forschungszentrum Jülich
102 PUBLICATIONS **1,980** CITATIONS
SEE PROFILE

THE JOURNAL OF PHYSICAL CHEMISTRY B

Article

pubs.acs.org/JPCB

Isothermal Behavior of the Soret Effect in Nonionic Microemulsions: Size Variation by Using Different *n*-Alkanes

Philipp Naumann,[†] Sascha Datta,[‡] Thomas Sottmann,*[,‡,⊥] Bastian Arlt,[†] Henrich Frielinghaus,[§] and Simone Wiegand*[,†,‡]

[†]ICS—Soft Condensed Matter, Forschungszentrum Jülich GmbH, D-52428 Jülich, Germany

[‡]Department für Chemie - Physikalische Chemie, Universität zu Köln, 50939 Cologne, Germany

[§]JCNS—Jülich Centre for Neutron Science, Forschungszentrum Jülich GmbH, D-52428 Jülich, Germany

[⊥]Institut für Physikalische Chemie, Universität Stuttgart, Pfaffenwaldring 55, 70569 Stuttgart, Germany

ABSTRACT: In this work we investigate the thermodiffusion behavior of microemulsion droplets of the type H_2O/*n*-alkane/$C_{12}E_5$ (pentaethylene glycol monododecyl ether) using the *n*-alkanes: *n*-octane, *n*-decane, *n*-dodecane, and *n*-tetradecane. In order to determine the thermodiffusion behavior of these microemulsion droplets, we apply the infrared thermal diffusion forced Rayleigh scattering (IR-TDFRS) technique. We measure the Soret coefficient (S_T) as function of the structure upon approaching the emulsification failure boundary (*efb*) and as a function of the radius of the spherical o/w microemulsion droplets close to the *efb*. By varying the chain length of the *n*-alkanes, we are able to study the thermodiffusion behavior of spherical o/w microemulsion droplets of different sizes at the same temperature. In the investigated range a linear dependence of the Soret coefficient as function of the radius was found. By use of a proposed relationship between the Soret coefficient and the temperature dependence of the interfacial tension, the transition layer *l* could be determined for the first time. Additionally, small angle neutron scattering (SANS) experiments are performed to determine the size and to prove that the shape of the microemulsion droplets is spherical close to the *efb*. Accordingly, the scattering curves could be quantitatively described by a combination of a spherical core−shell form factor and sticky hard sphere structure factor.

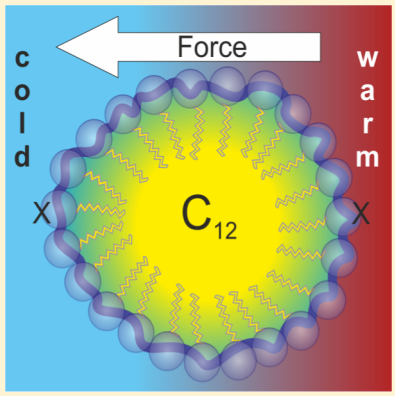

INTRODUCTION

Recently it has been demonstrated that thermal fields can be used to direct colloids and biomolecules to specific regions without requiring the use of lithographic structuring.[1] The underlying phenomenon is referred to as Soret effect. Thermodiffusion, akin to thermophoresis in colloidal dispersions, describes the mass transport in a mixture in the presence of a thermal gradient. A comprehensive microscopic description of the Soret coefficient S_T and the thermodiffusion coefficient, D_T, which can be expressed as the product of the mass diffusion coefficient, D, and, S_T, for liquids and colloidal dispersions is still not available. Many aspects such as the charge, mass, moment of inertia, and size dependence have been investigated experimentally and theoretically, and empirical correlations or agreement with theoretical models have been found for specific systems such as alkanes[2] or charged colloids,[3,4] but a general microscopic understanding has not been reached yet. One of the open questions is the size dependence of S_T, whether it is linear or quadratic.[5] While Duhr and Braun[6] observed an unambiguous quadratic dependence of S_T for carboxyl modified polystyrene (PS) beads in 1 mM Tris buffer of different radii in the range from 20 to 1000 nm using a microscopic fluorescence technique, studies by Putnam and Cahill of carboxyl functionalized PS spheres in a size ranging from 26 to 92 nm (PS) gave some indication that the behavior could also be linear. Later Vigolo et al.[7] obtained a linear dependence investigating bis(2-ethylhexyl)sulfosuccinate (AOT)/isooctane/water microemulsion droplets with a radius between 1.8 and 16 nm. Unfortunately the shape of the microemulsion droplets was not properly characterized, and thus, it is not certain that the microemulsion droplets are spherical in the range of study. Simultaneously the decreasing surface charge density of the AOT system with increasing radius will change the electrostatic contribution to the thermodiffusion properties. Recently, Braibanti et al.[8] repeated the experiment of Duhr and Braun[6] and studied the thermodiffusive behavior of highly diluted carboxyl modified PS spheres under the same conditions except that they used a 1:1 mixture of H_2O + D_2O to minimize sedimentation effects that can occur for the larger colloids. In the investigated radial range between 11 and 253 nm they found a linear size dependence for S_T. Also in theory the radial dependence is still controversially discussed. While Würger[9] expects a linear dependence for charged and uncharged solid colloids and

Received: December 11, 2013
Revised: February 25, 2014
Published: February 25, 2014

dx.doi.org/10.1021/jp412126n | *J. Phys. Chem. B* 2014, 118, 3451−3460

only for soft colloids a quadratic size dependence of S_T, Dhont et al.[10] also predict for charged solid colloids a quadratic dependence.

Very recently we studied the thermodiffusion behavior of H_2O/*n*-decane/$C_{12}E_5$ microemulsion following three different paths by changing the temperature, the oil content, and the volume fraction of the microemulsion droplets and investigated the relation between the interfacial tension and the Soret coefficient.[11] By adjustment of the appropriate concentration and temperature, a microemulsion forms discrete w/o or o/w aggregates, which are thermodynamically stable and can be used as colloidal model systems. Contrary to synthesized colloidal particles, radius and interfacial tension can be easily varied by temperature or composition.[12] We found only very small concentration effects on the thermodiffusion behavior below a volume fraction of 10%. By varying the oil content at a constant surfactant to water ratio, we were able to change the size of the microemulsion droplets at the *efb*, but simultaneously we also had to vary the temperature slightly so that the change in the Soret coefficient was not solely determined by size but also a temperature variation. In order to obtain microemulsions of different radius at isothermal conditions, in this work we studied the thermodiffusion behavior of microemulsion droplets by using different *n*-alkanes: *n*-tetradecane (*n*-C14), *n*-dodecane (*n*-C12), *n*-decane (*n*-C10), *n*-octane (*n*-C8), and a mixture (1:1) of *n*-octane/*n*-decane (*n*-C8/*n*-C10). Because of the fact that only the chain length of the *n*-alkane that is located inside the o/w droplets is changed, the surface properties are assumed to remain unaffected. Furthermore, we have chosen a nonionic surfactant to avoid charge effects.

We carefully characterized the phase behavior and studied the microstructure of the o/w microemulsions by SANS to eliminate perturbing effects that comprise results from earlier publications. The typical phase behavior of the investigated microemulsion systems is sketched in Figure 1. At low temperatures a coexistence of an oil-in-water microemulsion and an oil excess phase ($\underline{2}$) is found. With increasing temperature the so-called emulsification failure boundary (*efb*) is traversed and a thermodynamically stable, single phase microemulsion is formed. This one-phase region (1) closes like a funnel, when the *efb*, i.e., the capability of the surfactant to solubilize oil, intersects with the upper phase boundary ($1-\overline{2}$). This phase boundary originates from the cloud point curve of the binary system $H_2O/C_{12}E_5$ and is therefore often denoted as a near critical boundary (*ncb*).[13]

In contrast to colloidal dispersions containing hard spheres, microemulsions form a soft interface between water and oil established by the surfactant layer. The interfacial tension is strongly dependent on the curvature of the amphiphilic film which is temperature dependent. Thermodiffusion has already been associated with the so-called Marangoni effect.[18] In this work we are going to investigate the behavior compared to interfacial effects to find to which extent the interfacial tension influences the thermodiffusive behavior.

EXPERIMENTAL DETAILS AND CHARACTERIZATION

In this section we introduce the sample preparation and the experimental methods used. Furthermore we present the methods used to characterize the microstructure, i.e., dynamic light scattering (DLS) and small angle neutron scattering (SANS).

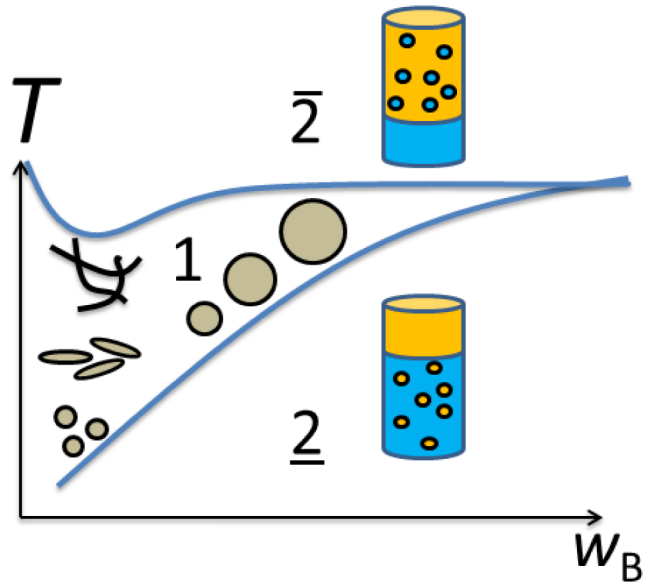

Figure 1. Schematic phase behavior of a water-rich microemulsion stabilized by a nonionic surfactant.[13] The phase boundaries are shown as a function of temperature and mass fraction w_B of the oil at a constant mass fraction γ_a of the surfactant in the mixture of water and surfactant. Between the lower emulsification failure boundary (*efb*) and the near critical boundary (*ncb*) a thermodynamically stable microemulsion is formed. Increasing the temperature results in a structural transformation from spherical droplets at the *efb* over elongated droplets to finally network like structures at the *ncb* before demixing occurs.[14−17] Increasing the mass fraction of oil and temperature staying at the *efb* will yield larger microemulsion droplets.

Sample Preparation. The surfactant pentaethylene glycol monododecyl ether ($C_{12}E_5$, purity of ≥99%) and the various *n*-alkanes (purity of ≥99%) were each purchased from Sigma-Aldrich and used without further purification. The water was obtained from a Milli-Q dispenser. D_2O (purity of ≥99%) and deuterated *n*-alkanes were acquired from Euriso-top. The samples were prepared by weighting the appropriate amount of water, m_A (usually around 2 g) and then adding the required amount of surfactant (m_C) and afterward the corresponding amount of oil (m_B). The target composition was achieved within an accuracy of 2 mg. Identical compositions of protonated samples (phase behavior, DLS, TDFRS) and deuterated samples (SANS) were prepared with respect to molar fractions, i.e., volume fractions which are summarized in Table 1 were calculated using the respective densities. The sample was then inserted into a bath of thermostated water to determine the phase behavior, i.e., the location of the phase boundaries. Both DLS and thermodiffusion samples were filtered in the one-phase state by a Pall-Acrodisc syringe filter with a pore size of 0.8/0.2 μm. For the SANS measurements we

Table 1. Composition of the Studied Microemulsions[a]

n-alkane	Φ_C	$\Phi_{C,i}$	Φ_B
n-C8	0.028	0.027	0.084
n-C8/*n*-C10 (1:1)	0.029	0.028	0.060
n-C10	0.029	0.029	0.040
n-C12	0.030	0.029	0.026
n-C14	0.030	0.030	0.017

[a]Given are the volume fractions of the surfactant Φ_C, the surfactant in the internal interface $\Phi_{C,i}$ and the oil Φ_B.

dx.doi.org/10.1021/jp412126n | J. Phys. Chem. B 2014, 118, 3451−3460

used Hellma quartz cells with an optical path length of 1 mm. For the IR-TDFRS measurements, the sample was put into Hellma quartz cells with a thickness of 0.2 mm which was sealed with Teflon stoppers. Note that during the filling, the sample was in the single phase state and the measurement cell was also kept at the same temperature to avoid phase separation. Finally, the cell was placed into a thermostated holder inside an infrared thermal diffusion forced Rayleigh scattering (IR-TDFRS) setup.[19]

Refractive Index Increments. To determine the refractive index increment with concentration $(\partial n/\partial c)_{T,p}$, we used an Abbe refractometer by Anton Paar.[20] Samples of different concentrations were repeatedly inserted into the refractometer at different temperatures over the necessary temperature range. Each refractive index value was determined at least five times. We measured the increment each in the vicinity around the sample concentration probed in thermodiffusion measurements. Typical values of $(\partial n/\partial c)_{T,p}$ spread from 0.110 to 0.116 with an accuracy of 5×10^{-5}. The refractive index increment with temperature $(\partial n/\partial T)_{c,p}$ was obtained in an interferometric setup,[21] upon measurement of the phase shift between the sample and the reference beam while the temperature of the sample was increased or decreased linearly over the typical measurement range. The value of $(\partial n/\partial T)_{c,p}$ varies between 1.20×10^{-4} K^{-1} and 1.50×10^{-4} K^{-1} with a typical accuracy of 5×10^{-6} K^{-1}. The measurements were only conducted at the concentrations probed in the thermodiffusion measurements.

Small Angle Neutron Scattering. SANS measurements were carried out using the instrument KWS 1 at the Jülich Centre for Neutron Science (JCNS), hosted at the Research Neutron Source Heinz Maier-Leibnitz (FRM II) in Garching, Germany. Samples were placed in the quartz cells which were equilibrated to the desired temperature in a home-built cell holder with an accuracy of ±0.05 K. Data were collected at wavelengths of λ = 4.8 and 12.0 Å with a wavelength distribution of the velocity selector of $\Delta\lambda/\lambda$ = 0.20 (full width at half-maximum). Measurements were performed at sample-to-detector distances of 2 and 8 m, thereby covering a wide range of the scattering wave vector $q = (4\pi/\lambda)\sin(\theta/2)$ with the scattering angle θ. Collimation and aperture settings were chosen in order to optimize the neutron flux without exceeding the detector capacity. The raw data were radially averaged and normalized according to standard procedures using the program QtiKWS provided by the JCNS. Plexiglas of 1.5 mm path length was used as absolute calibration standard.

The experimental scattering curves were analyzed assuming a collection of spherical particles in solution. By application of the decoupling approximation,[22] the scattering intensity $I(q)$ as function of the scattering vector q can be written as

$$I(q) = nP(q)S(q) + I_{\text{incoh}} \tag{1}$$

Therein the form factor $P(q) = [A(q)]^2$ is the square of the scattering amplitude A of the scattering particles, and $S(q)$ is the structure factor describing the interaction of the particles. n is the number density of the particles. Polydispersity is taken into account by convoluting the form factor with a Gaussian size distribution $W(R,R_0,\sigma)$ with the mean radius R_0 and the standard deviation σ. The scattering intensity is then given by

$$I(q) = nS(q)\int_0^\infty P(q, R)W(R, R_0, \sigma)\,\mathrm{d}R + I_{\text{incoh}} \tag{2}$$

In order to describe the experimental scattering data, we used the form factor of a Gaussian shell with diffuse interface and core scattering,[23] given by

$$\begin{aligned} P(q) &= [A(q)]^2 \\ &= \Delta\rho_{\text{core}}^2 V_{\text{core}}^2 A_{\text{core}}^2(q) + \Delta\rho_{\text{film}}^2 V_{\text{film}}^2 A_{\text{film}}^2(q) \\ &\quad + 2\Delta\rho_{\text{core}}\Delta\rho_{\text{film}} V_{\text{core}} V_{\text{film}} A_{\text{core}}(q) A_{\text{film}}(q) \end{aligned} \tag{3}$$

Hereby the scattering amplitude of the core is the well-known (normalized) amplitude of a homogeneous sphere,[24]

$$A_{\text{core}}(q) = \frac{4\pi}{q^3 V_{\text{core}}}\{\sin(qR) - qR\cos(qR)\} \tag{4}$$

with V_{core} being simply the volume of a sphere with radius R. The scattering amplitude of the surfactant film was given by Gradzielski et al.,[25]

$$A_{\text{film}}(q) = \frac{4\pi l_C}{qV_{\text{film}}}\exp\left\{\frac{-q^2t^2}{2}\right\}\{qt^2\cos(qR) - R\sin(qR)\} \tag{5}$$

with $V_{\text{film}} = 2\pi(4Rt^2 + l_C(t^2 + R^2))$ being the volume of the surfactant film. Thereby t is a measure for the thickness of the diffuse amphiphilic film and $l_C \approx v_C/a_C$ is the length of a surfactant molecule, given by the ratio of the volume v_C and the headgroup area a_C of the surfactant molecule. The contrasts are considered by the scattering length density differences $\Delta\rho_{\text{core}} = \rho_{\text{bulk}} - \rho_{\text{core}}$ and $\Delta\rho_{\text{film}} = \rho_{\text{bulk}} - \rho_{\text{film}}$, respectively. With inclusion of the polydispersity according to eq 2, the scattering intensity of the noninteracting droplets ($S(q) = 1$) is expressed by

$$I(q) = I_{\text{core}}(q) + I_{\text{film}}(q) + I_{\text{cross}}(q) \tag{6}$$

The three contributions are given in large detail in ref 23. The free parameters of this model are the mean radius R_0, the thickness of the diffuse amphiphilic film t, and the standard deviation of the polydispersity distribution σ.

Dynamic Light Scattering. In dynamic light scattering (DLS) experiments the intensity fluctuations are measured at a detector at a certain scattering angle θ that corresponds to a scattering wave vector $q = (4\pi n/\lambda)\sin(\theta/2)$, with the refractive index, n, and the wavelength, λ. We used a commercially available instrument (ALV/SP-86 no. 059) with a helium−neon laser at a wavelength λ = 633 nm. Cylindrical sample cells were chosen, which were placed in a thermostated toluene bath with a temperature stability of ΔT = ±0.05 K. The scattering intensity $I(q,t)$ was detected with a photomultiplier at angles $30° \le \theta \le 150°$ and was analyzed by the correlator card (ALV3000). Further processing was performed using the program package BATCON, which contains as an essential feature the program package CONTIN[26] in order to extract the intensity autocorrelation function as well as the distribution function $A(\Gamma)$ of the inverse relaxation times Γ.

Infrared Thermal Diffusion Forced Rayleigh Scattering. The infrared thermal diffusion forced Rayleigh scattering (IR-TDFRS) is optimized for aqueous systems and utilizes a weak absorption band of water in the infrared to create a temperature gradient. Details can be found elsewhere.[19,27] Two infrared laser beams are crossed and create a sinusoidal interference grating. Because of absorption of the IR light by the aqueous sample, the intensity grating is transformed into a temperature grating. For all investigated microemulsions in this

dx.doi.org/10.1021/jp412126n | J. Phys. Chem. B 2014, 118, 3451−3460

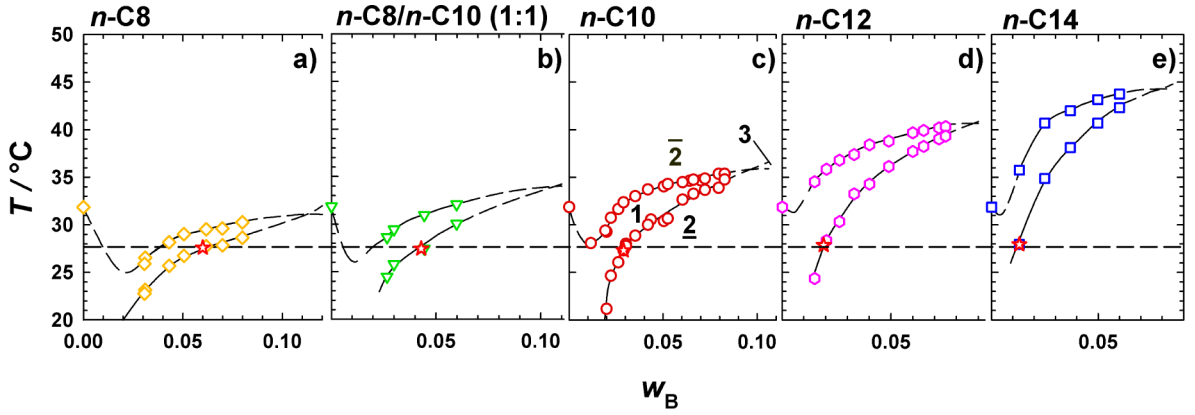

Figure 2. Phase behavior of water-rich microemulsion systems of the type H_2O/*n*-alkane/$C_{12}E_5$ at a constant mass fraction of $C_{12}E_5$ in the H_2O/$C_{12}E_5$ mixture $\gamma_a = 0.03$. The microstructure and the thermal diffusion behavior has been studied near the *efb* at $T_{efb} = 27.0 \pm 0.5$ °C (stars, connected by the dashed dotted line). With an increase of the chain length of the *n*-alkane, the one phase region shifts to higher temperatures. Concomitantly, the maximum amount of oil that can be solubilized at $T = 27.0 \pm 0.5$ °C decreases strongly.

work thermodiffusion forced the microemulsion droplets toward the cold side. The temperature and concentration changes lead to a modulation of the refractive index, which is probed by an additional readout laser. The alteration in the refractive index grating leads to a change of the intensity of this diffracted beam. The intensity change as function of time was monitored by an avalanche diode. Note that the local heating of the sample cell due to the IR laser must be taken into account in order to compare the results with DLS, SANS, and phase diagram measurements.

RESULTS

Phase Behavior. The phase behavior of water-rich microemulsions of the type H_2O/*n*-alkane/pentaethylene glycol monododecyl ether ($C_{12}E_5$) is studied as a function of temperature and the overall weight fraction w_B of *n*-alkane at a constant ratio of $\gamma_a = m_C/(m_C + m_A) = 0.03$. Figure 2 shows the $T(w_B)$ sections obtained using *n*-C8, *n*-C8/*n*-C10 (1:1), *n*-C10, *n*-C12, and *n*-C14, respectively, as *n*-alkanes. In all cases a sequence of phases is found that is typical for nonionic microemulsion systems.[13] As can be seen, by decrease of the chain length of the *n*-alkane, the intersection point of the *efb* and *ncb* shifts to lower temperatures and larger weight fractions w_B. By comparison of the maximum amount of *n*-alkane that can be solubilized at a constant temperature of $T_{efb} = 27.0 \pm 0.5$ °C, an increase by more than a factor of 4 is found as the chain length decreases (cf. stars in Figure 2). Accordingly the size of the droplets will also increase when the chain length of the oil is reduced.

Microstructure. The variation of the microstructure in the one-phase region of water-rich microemulsions has been both experimentally and theoretically studied.[14−17] In order to ensure the spherical shape of the o/w microemulsion droplets and to determine their radius, small angle neutron scattering experiments were performed in the vicinity of the *efb* for each system at 26.1 ± 0.4 °C. Thereby film contrast conditions were adjusted by using adequate mixtures of protonated and deuterated *n*-alkanes in order to match the scattering length density of the droplet core with scattering length density of the surrounding D_2O ($\rho_{bulk} = \rho_{core}$). However, the quantitative analysis of the scattering data (see below) showed that $\rho_{bulk} \neq \rho_{core}$, i.e., that the scattering from the droplet core had to be taken into account. Obvious reasons for this mismatch are the fact that we did not include the monomeric solubility of the protonated surfactant in the *n*-alkanes[28] as well as undeuterated impurities in the deuterated species in the calculation of the scattering length densities ρ. The inset in Figure 3a shows the radial scattering length density profile exemplary by means of the *n*-octane microemulsion. As can be seen, the scattering length densities of core and bulk are only slightly different. Furthermore, the parameter t (measure of the thickness of the

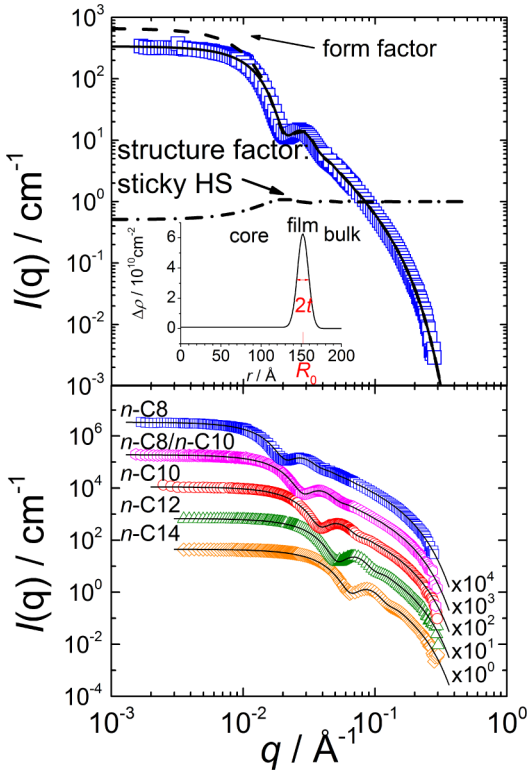

Figure 3. SANS measurement performed in film contrast to determine the size and shape of the microemulsion aggregates at the corresponding *efb* temperature. The scattered intensity is plotted versus the scattering vector q. The data are described by an appropriate combination of form and structure factor. The inset in part a (top) shows the radial scattering length density profile of the system *n*-octane. See text for details.

dx.doi.org/10.1021/jp412126n | J. Phys. Chem. B 2014, 118, 3451−3460

diffusive amphiphilic film), which will later be compared to the thickness l of the transition layer, is schematically depicted. Note that the *efb* is shifted to $T_{efb} = 26.1 \pm 0.4$ °C, i.e., by 0.9 K to lower temperatures, using deuterated instead of protonated solvents which is in agreement with literature.[29] The scattering curves obtained are shown in Figure 3 after subtraction of the incoherent background scattering intensity. All curves resemble the typical scattering pattern of spherical shells and a small fraction of core scattering;[23] i.e., the scattering intensity is almost constant at low values of the scattering vector q. When q is increased, the intensity decreases steeply until the first minimum is reached. At large values of q the intensity decreases with an $\exp(-q^2t^2)q^{-2}$ dependence as a result of the diffuse nature of the amphiphilic film.[25] By comparison of the scattering curves shown in Figure 3b, it is evident that the position of the minimum, which is related to the radius of the shells ($R \approx \pi/q$) shifts systematically to lower values of q if the chain length of the solubilized *n*-alkane is decreased.

In Figure 3a the scattering curve of the microemulsion containing *n*-octane (*n*-C8) is exemplarily shown. As can be seen, the description of the scattering data solely by the form factor given by eq 6 (represented by the dashed line), which neglects the contribution of any interaction (i.e., assuming $S(q) = 1$), led to higher scattering intensities at low values of q, which indicates the presence of interdroplet interactions. These interactions are the largest for the *n*-C8 system and become less significant for the microemulsions containing longer *n*-alkanes, i.e., with decreasing droplet volume fraction. In order to account for these interactions, we used the structure factor of hard spheres with surface adhesion (sticky hard spheres).[30,31] Note that the Percus−Yevick model for hard spheres could not describe the scattering intensity quantitatively. The structure factor for hard spheres with surface adhesion (sticky hard spheres)[30] as given by Menon et al.[31] is

$$S(x) = A^{-2}(x) + B^{-2}(x) \tag{7}$$

where $x = aq$ with $a = \delta + \Delta$. δ represents the inner hard core diameter of the particle, and Δ is the thickness of the attractive well of the potential of depth u_0. Δ was set equal to t and a was set to $a = 2(R_0 + t)$ in order to reduce the number of free parameters. With the relative thickness of the attractive well $\epsilon = \Delta/a$ the so-called stickiness parameter τ of the potential is defined by

$$\tau = (12\epsilon)^{-1}\exp[u_0/(kT)] \tag{8}$$

The terms $A(x)$ and $B(x)$ are given by

$$A(x) = 1 + 12\eta\left\{\alpha\left[\frac{\sin(x) - x\cos(x)}{x^3}\right] + \beta\left[\frac{1-\cos(x)}{x^2}\right] - \frac{\lambda}{12}\frac{\sin(x)}{x}\right\} \tag{9}$$

and

$$B(x) = 12\eta\left\{\alpha\left[\frac{1}{2x} - \frac{\sin(x)}{x^2} + \frac{1-\cos(x)}{x^3}\right] + \beta\left[\frac{1}{x} - \frac{\sin(x)}{x^2}\right] - \frac{\lambda}{12}\frac{1-\cos(x)}{x}\right\} \tag{10}$$

with

$$\alpha = \frac{(1 + 2\eta - \mu)}{(1-\eta)^2}, \quad \beta = \frac{(-3\eta + \mu)}{2(1-\eta)^2} \tag{11}$$

and $\mu = \lambda\eta(1 - \eta)$. $\eta = \phi_{disp}\, a^3/\delta^3$ is the effective volume fraction of the spheres and λ the smaller solution of quadratic equation

$$\lambda^2 - 12\left(\frac{\tau}{\eta} + \frac{1}{1-\eta}\right)\lambda + \frac{12 + 6\eta}{\eta(1-\eta)^2} = 0 \tag{12}$$

Accordingly the only free parameter of this model is the depth of the attractive potential well u_0. By using the combination of both form factor (dashed line) and structure factor (dashed-dotted line), the experimental scattering intensities could be quantitatively described for all systems. The parameters obtained are compiled in Table 2. As can be seen, the radius

Table 2. Fit Parameters of the Form and Structure Factor Applied To Describe the SANS Curves of the Water-Rich Microemulsions D_2O/*n*-Alkane/$C_{12}E_5$ with the Composition Given in Table 1 at $T_{efb} = 26.1 \pm 0.4$ °C [a]

n-alkane	R_0, nm	σ, nm	t, nm	ϵ	η	$-u_0$, kT
n-C8	15.2 ± 0.3	2.8	0.6	0.021	0.117	1.52
n-C8/*n*-C10 (1:1)	11.0 ± 0.3	1.9	0.6	0.029	0.095	1.23
n-C10	8.1 ± 0.2	1.3	0.6	0.037	0.077	0.91
n-C12	6.0 ± 0.1	0.9	0.6	0.049	0.064	0.76
n-C14	4.7 ± 0.1	0.7	0.6	0.061	0.057	0.67

[a]Note that the temperature in SANS experiments was slightly lower because of the deuterated solvents. Listed are the mean droplet radius R_0, standard deviation of the polydispersity distribution σ, thickness of the diffuse amphiphilic film t, relative thickness of the attractive potential well $\epsilon = \Delta/a = t/2(R_0 + t)$, effective droplet volume fraction $\eta = \Phi_{disp}a^3/\delta^3 = \Phi_{disp}\,((2R_0)/2(R_0 + t))^3$, and potential depth u_0.

R_0 of the microemulsion droplets increases from $R_0 = 4.7$ to $R_0 = 15.2$ nm if the chain length of the *n*-alkane is reduced. At the same time the polydispersity index $p = \sigma/R_0$ increases slightly from 0.15 to 0.18. The thickness t of the diffuse amphiphilic film was found to be $t = 6$ Å for all microemulsion systems under study, i.e., independent of the chain length of the solubilized *n*-alkane. A somewhat smaller value of $t = 5$ Å was found for water-in-cyclohexane microemulsions stabilized by $C_{12}E_6$.[32] Furthermore the depth of the attractive potential well u_0 becomes deeper, indicating that the effect of surface adhesion increases in case the chain length of the alkane decreases (i.e., the droplet radius is enlarged) via a weakening of the hydrogen bonds.

In order to monitor the size of the microemulsion droplets as a function of temperature, we performed DLS measurements at different temperatures between the *ncb* and the *efb*. Figure 4 shows the hydrodynamic radius R_H, which has been derived from the diffusion coefficient D using the Stokes−Einstein relation for different temperatures. It can be seen that R_H increases with temperature approaching the *ncb*, and for all temperatures the diffusion of the microemulsions aggregates becomes faster with increasing chain length of the *n*-alkanes. The analysis of the data using the Stokes−Einstein relation, however, is only justified close to the *efb*, where the droplets are spherical.[33] At higher temperatures it is known that the droplets elongate and form network-like structures close to the *ncb*.[14−17]

dx.doi.org/10.1021/jp412126n | J. Phys. Chem. B 2014, 118, 3451−3460

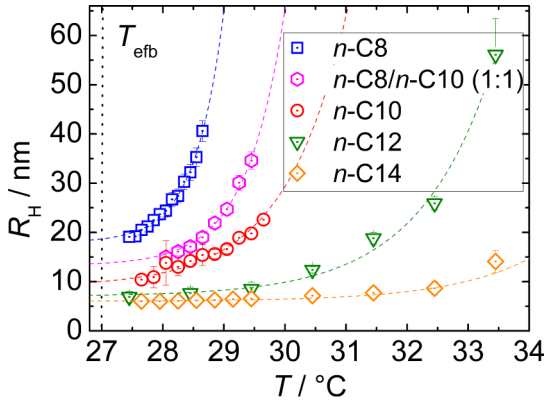

Figure 4. Hydrodynamic radius, R_H, as a function of temperature for microemulsion with various *n*-alkanes and *n*-alkane mixtures determined by DLS. The composition of the samples is given in Table 1.

Thermodiffusion Behavior. We studied the thermodiffusion behavior of the microemulsions with *n*-C8, *n*-C8/*n*-C10 (1:1), *n*-C10, *n*-C12, and *n*-C14 as a function of the temperature in the one-phase region and as function of w_B by changing the oil component at constant temperature. As illustrated in Figure 2, we can compare the measurements for different *n*-alkane microemulsions at the same *efb* temperature, which ensures, as shown by SANS, spherical droplets with different sizes depending on the chain length of the *n*-alkane. At this point we assume that the interactions between the microemulsion droplets are dominated by the surfactant molecules.

Temperature Dependence. In order to study the temperature dependence we performed measurements within the one-phase region, above the *efb* and below the *ncb*.[11] The transition from the one-phase region to the 2-phase region is kinetically hindered so that measurements in the 2-phase region were possible before the phase separation sets in. Figure 5 shows the collective diffusion D, thermodiffusion D_T, and Soret coefficient S_T in the one-phase region for the five microemulsions under study as a function of temperature. The diffusion coefficient D shows two linear regimes with different slopes. It increases significantly, when the temperature is lowered, because the droplets become smaller and almost spherical in shape. For *n*-tetradecane the thermodiffusion coefficient D_T first reduces with cooling from the *ncb* and reaches a minimum. Further decrease of temperature results in a steep increase of the thermodiffusion coefficient D_T until it becomes almost constant for temperatures close to the *efb*. As a reminder, in this temperature range the microemulsion droplets are spherical and constant in size. The Soret coefficient S_T, the quotient of the thermal and collective diffusion coefficient, behaves almost like the thermodiffusion coefficient. When the temperature decreases from the *ncb*, S_T decreases steeply going through a minimum and a plateau value is reached just below or in the vicinity of the *efb* temperature. Also, for the shorter *n*-alkanes we would expect a minimum as was observed for *n*-C14, but because of the smaller width of the one-phase region, it was difficult to detect. Especially for the microemulsion containing tetradecane it is obvious that the value of S_T is constant for a rather wide temperature range of 3−4 K because the particle radius does not change. It seems to be likely that the transition from a network structure to individual droplets corresponds to a minimum in the thermodiffusion properties.

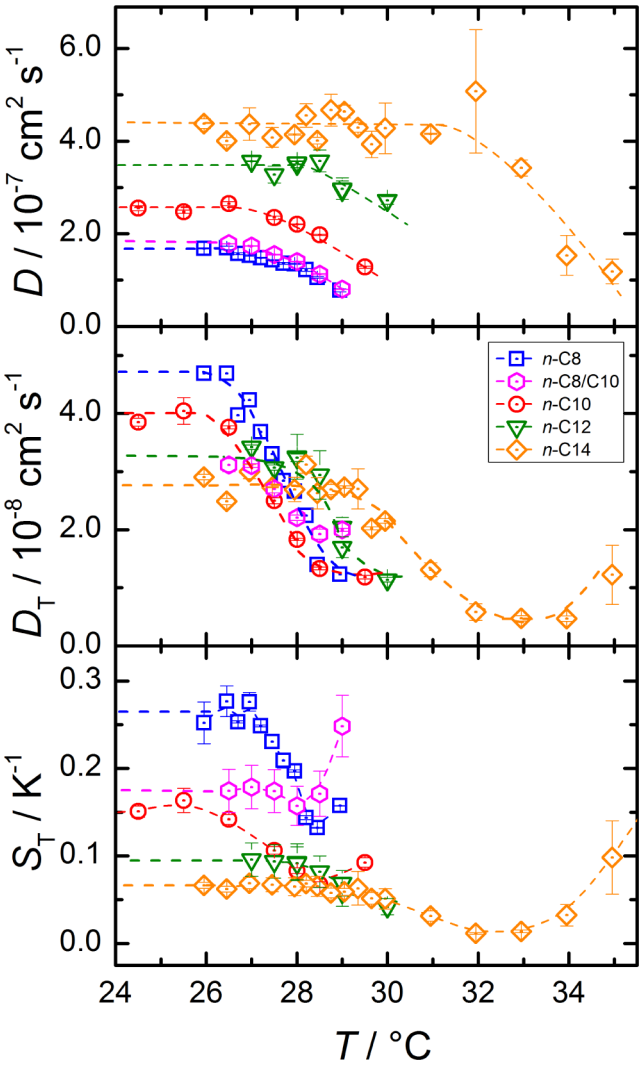

Figure 5. Diffusion D, thermodiffusion D_T, and Soret coefficient S_T as a function of temperature. The five microemulsion systems (compositions are given in Table 1) are studied in the one-phase region. We used the same symbols as in Figures 2−4, and the dashed lines are guides to the eye.

The measurements of the *n*-C8 system were complicated because of a very narrow one-phase region so that the range in which spherical droplets exist was rather small and additionally the volume fraction of the droplet concentration was already 11.7%. But in the earlier work we have shown that interaction effects can still be neglected[11] and the thermodiffusive behavior is mainly determined by size effects and not by interactions.

Size Dependence. As mentioned above in this work, we study the radial dependence of the thermodiffusion properties of microemulsion droplets at a constant temperature of T = 27.0 °C by varying the *n*-alkane chain length from *n*-tetradecane down to *n*-octane. To obtain the transport coefficients close to the *efb*, we extrapolated the values measured as a function of temperature toward the *efb*. Figure 6 shows the extrapolated D, D_T, and S_T values for the five microemulsions with different oil components as a function of $R_{SANS} = R_0 + t$, which corresponds to an apparent smaller radius compared to the one obtained by dynamic light scattering (R_H).

The diffusion coefficient, D, decreases with increasing radius of the microemulsion droplets. The thermodiffusion coefficient,

dx.doi.org/10.1021/jp412126n | J. Phys. Chem. B 2014, 118, 3451−3460

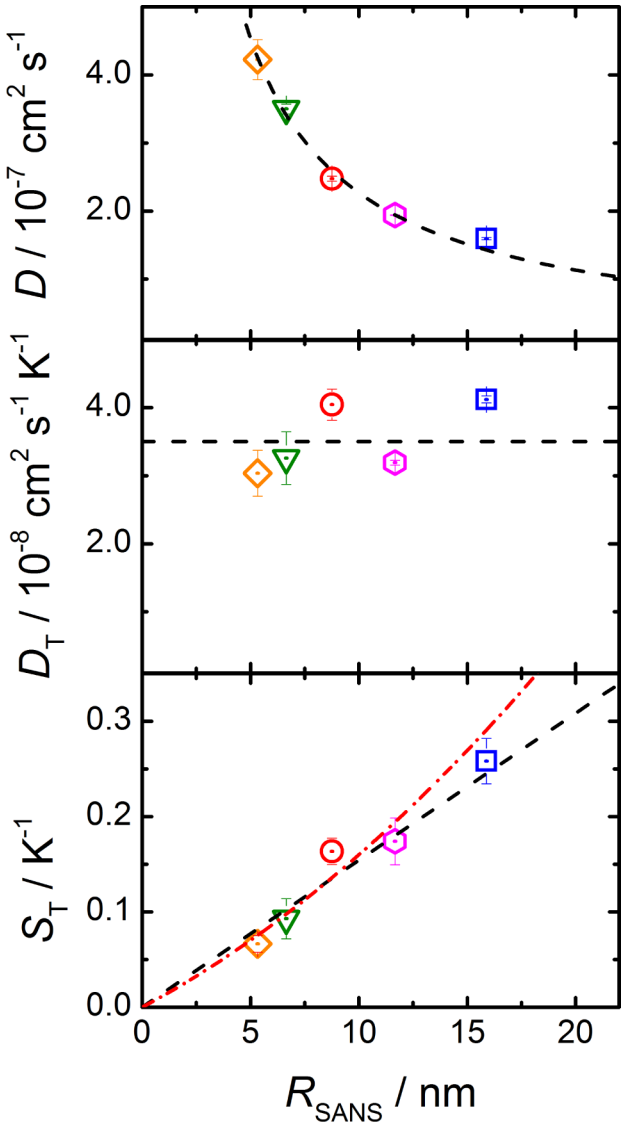

Figure 6. Diffusion D, thermodiffusion D_T, and Soret coefficient S_T for the five microemulsions under study extrapolated to the *efb* temperature of 27.0 °C as a function of $R_{SANS} = R_0 + t$ with the core radius R_0 and the thickness of the diffuse amphiphilic film t. We used the same symbols as before. For D the black line is a $1/R_0$ fit. For D_T it is a constant. For S_T the black line is a linear fit and the red dash dot line is a parabolic fit.

D_T, seems independent of the droplet radius, while the Soret coefficient is proportional to the radius. For this size range from around 5 to 16 nm, a linear increase of S_T with R_{SANS} with a slope of 0.016 K^{-1} nm^{-1} is observed.

Compared to the approach we used for the *n*-decane system,[11] we could avoid a simultaneous change of the temperature while the radius is varied. As seen in Figure 2, we increase the oil fraction and thus the radius but keep the *efb* temperature constant. On the other hand the drawback of this scenario is different oil components, which modify the core of the microemulsion droplets. But because of the fact that we use only linear *n*-alkanes, which vary rather regularly[2] and have similar interactions compared with the surfactant molecules, we do not expect an influence on the thermodiffusion. This would probably be different if we would use branched alkane isomers because for those molecules a clear dependence of the thermodiffusive behavior on the molecular structure has been reported.[34]

Interfacial Tension. Already from the early work by the Giddings group,[35] it is known that the surface groups of colloidal particles change the thermodiffusion behavior substantially, indicating that the interface between the solute particle and the solvent is an important factor. Later Piazza and Parola[36] related the Soret coefficient of a colloid with radius R to the temperature derivative of the product of the interfacial tension σ_{ab} and a characteristic length l,[36] which has been initially related to the interaction range between the colloid and the solvent and later to the width of a fluid layer, where the pressure tensor is asymmetric,[5] in the following way:

$$S_T = \frac{4\pi R}{k_B T}\frac{\partial(l\sigma_{ab})}{\partial T} \tag{13}$$

Applied to the systems under study, this equation might be understood intuitively with the help of Figure 7, which schematically shows the microemulsion droplet in a temperature gradient. Inside it contains the oil, and the interface

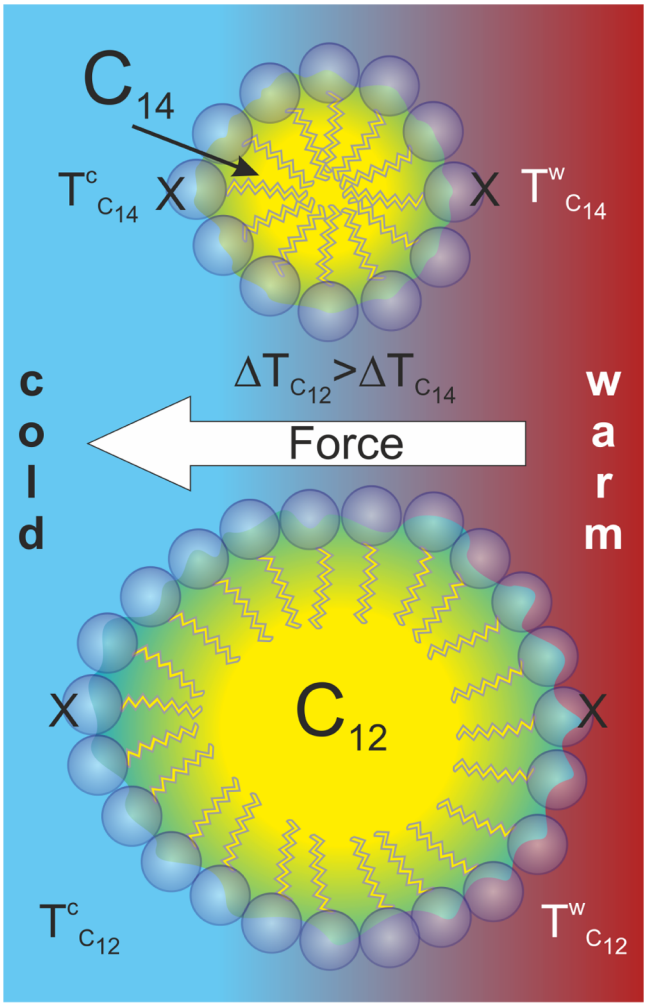

Figure 7. Qualitative illustration of eq 13. Exemplarily we show schematically two microemulsion droplets solubilizing *n*-tetradecane and *n*-dodecane, respectively. The blue circles represent the hydrophilic headgroups. Because of the larger droplet size for the shorter oil, the temperature difference between both sides of the droplet marked by "x" is also larger. For further details, see the text.

dx.doi.org/10.1021/jp412126n | J. Phys. Chem. B 2014, 118, 3451−3460

between water and the oil is formed by a surfactant layer, which is partially penetrated by oil and water from the inside and outside, respectively. The force acting on the soft colloid depends on the distance 2*R* between the two points marked by "x" lying in the warm and cold region. According to eq 13, we expect a larger S_T in the case of *n*-octane due to its larger droplet size, which is confirmed in Figure 6 (bottom). Additionally, the thermophoretic force also depends on the temperature dependence of the interfacial tension σ_{ab} and the thickness *l*. The change of the interfacial tension with temperature is indicated in Figure 7 by a slight asymmetry of the droplet (cf. droplet with *n*-dodecane). The increasing interfacial tension σ_{ab} with decreasing temperature leads to a higher curvature equal to a smaller radius on the cold side. As already mentioned, the definition of *l* is ambiguous; sometimes[36] it is interpreted as a measure of the range of the colloid−solvent interaction and otherwise[5] as the width of the fluid layer with an anisotropic pressure tensor also denoted as transition layer. Regarding the range of interactions and considering only short-range van der Waals interactions, we expect *l* in a range of 1−2 Å. If we follow the fluid layer argument, it might be possible to identify *l* with the thickness of the diffuse amphiphilic film *t* in the order of 6 Å.

Accordingly, we expect a larger S_T with a growing particle radius, *R*, and an increasing temperature sensitivity of the interfacial tension σ_{ab} and the thickness *l*. Because of the almost linear dependence of S_T on the radius, both dependencies almost cancel out.

On the basis of this approach, we compared in a recent study the interfacial tension data of the *n*-decane microemulsion with the measured Soret coefficients[11] and found some consistency with this approach. Now we can extend our comparison to microemulsions containing different *n*-alkanes. Most of the interfacial tension data have been measured by Sottmann and Strey[37] by the so-called spinning drop technique.[38] In this study we measured the interfacial tension of the system *n*-C8/*n*-C10 (1:1) in the relevant temperature regime between 25.5 and 29.6 °C. To validate our data, we additionally repeated some of their data points. Figure 8 shows the interfacial tension as function of the temperature on a logarithmic scale and in the inset on a linear scale. The oil/water interfacial tension is known to run through a pronounced minimum at the phase inversion temperature of the respective system.[39]

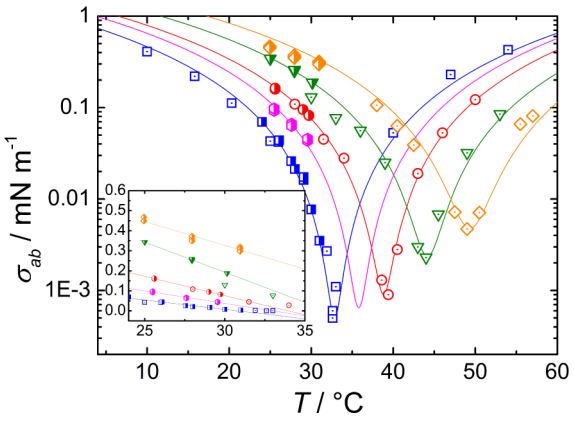

Figure 8. Oil/water interfacial tension of the system H_2O/*n*-alkane/$C_{12}E_5$ as a function of temperature. The inset shows σ_{ab} on a linear scale in the investigated temperature range. The open symbols refer to Sottmann et al.,[37] and the semidouble symbols have been measured in this work. The shape of the symbols characterizes the system and is identical with the previous figures.

While over the entire temperature range a parabolic temperature dependence is found,[12,40,41] the temperature derivative stays almost constant in the investigated range. In the inset it becomes obvious that the temperature derivative of the interfacial tension is negative and varies with the chain length of the *n*-alkanes. The absolute value increases with the chain length of the *n*-alkane so that forces generated due to the difference in the interfacial tension become larger, but simultaneously the radius of the droplet also decreases (cf. Tables 3 and 2). According to eq 13, we expect a negative Soret coefficient, which is not found experimentally, so that we consider in the following only the absolute value of $(\partial\sigma_{ab}/\partial T)$.

Table 3. Interfacial Tension Derivatives with Respect to Temperature for Microemulsions Containing *n*-Alkanes, the Thickness of the Transition Layer *l* (Neglecting Its Temperature Dependence) Derived from Eq 13, and $R_{SANS} = R_0 + t$ at the *efb*

n-alkane	$\lvert\partial\sigma_{ab}/\partial T\rvert/10^{-3}$ N/(K m)	*l*/nm	R_{SANS}/nm
n-C8	0.0093	0.6	15.9
n-C8/*n*-C10 (1:1)	0.0125	0.3	11.7
n-C10	0.0214	0.3	8.8
n-C12	0.0313	0.2	6.7
n-C14	0.0421	0.1	5.3

If we assume that the thickness of the transition layer *l* does not depend on temperature, we can determine $l = (k_BT/(4\pi R_{SANS}))S_T/(\partial\sigma_{ab}/\partial T)$ from eq 13 using the Soret coefficient S_T and the radius R_{SANS} measured at the *efb*. This leads to the *l*-values listed in Table 3. Note that *l* is of the same order of magnitude as the thickness of diffuse interfaces in microemulsion systems for the microemulsions containing *n*-octane.[25,29] Additionally, we observe that *l* decreases with increasing length of the *n*-alkane chain while the thickness of the diffusive interface *t* determined in the SANS experiments (cf. Table 2) stays constant.

If we use the data summarized in Table 3 and look at the results of the microemulsions with different *n*-alkanes and analyze the dependence of $S_T^{n\text{-alkane}}$ versus the product of $R_{SANS}^{n\text{-alkane}}$ and $\lvert(\partial\sigma_{ab}/\partial T)\rvert$, we can in principle determine an averaged thickness of the transition layer *l* using eq 13, which describes all microemulsions. Although we find a linear dependence between $S_T^{n\text{-alkane}}$ and the product, the line does not go through the origin as expected from eq 13. The inconsistent picture is probably a shortcoming of our original assumption that *l* is temperature independent.

Therefore, we included the temperature dependence of *l*, which leads to

$$\frac{k_BT}{4\pi R_{SANS}(T)}S_T(T) = \underbrace{l\left(\frac{\partial\sigma_{ab}}{\partial T}\right)}_{\text{intercept}} + \left(\frac{\partial l}{\partial T}\right)\sigma_{ab}(T) \qquad (14)$$

In Figure 9 we plot the left side of eq 14 versus the temperature dependent interfacial tension $\sigma^{n\text{-alkane}}(T)$ for the different microemulsions. Note that we use the values of S_T and R_H measured in the one-phase region at different temperatures. We find a linear dependence for all systems. From the slope we can determine $(\partial l/\partial T)^{n\text{-alkane}}$, and $l^{n\text{-alkane}}$ can be obtained from the intercept after dividing by $(\partial\sigma_{ab}/\partial T)^{n\text{-alkane}}$. Following this procedure we determine *l* to be in the angstrom range. Note

dx.doi.org/10.1021/jp412126n | J. Phys. Chem. B 2014, 118, 3451−3460

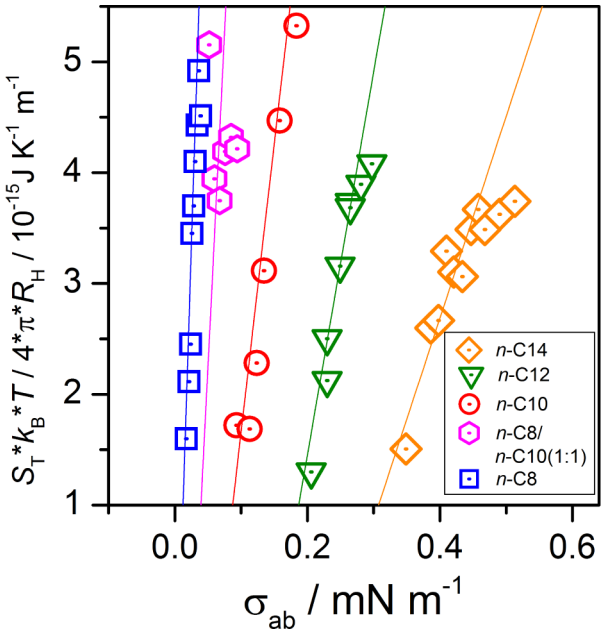

Figure 9. Plot of the left side of eq 14 versus the interfacial tension $\sigma_{ab}^{n\text{-alkane}}$ of the microemulsions with the different *n*-alkanes.

that the uncertainty of l is quite high in the range of 20−50%. The variation of l with temperature is in the "per thousand" range and shrinks with the droplet size, which is quite reasonable (cf. Table 4).

Table 4. Thickness of the Transition Layer l and $(\partial l/\partial T)$ according to eq 14, which Includes the Temperature Dependence of l

n-alkane	$l^{n\text{-alkane}}$/nm	$(\partial l/\partial T)^{n\text{-alkane}}/10^{-13}$ m K^{-1}
n-C8	0.14 ± 0.06	1.87 ± 0.20
n-C8/*n*-C10 (1:1)	0.19 ± 0.05	1.20 ± 0.13
n-C10	0.16 ± 0.04	0.52 ± 0.06
n-C12	0.17 ± 0.03	0.35 ± 0.04
n-C14	0.11 ± 0.02	0.18 ± 0.02

We can conclude that for the system under investigation an increase of l from 0.1 to 0.6 nm with decreasing chain length of the oil is found by applying the model and neglecting the temperature dependence of l (cf. Table 3). On the other hand, including the temperature dependence of l leads to a constant value between 0.1 and 0.2 nm. Although the physical origin of the l-parameter is not very well-defined, we find in the present analysis rather small values for l, which correspond to typical van der Waals radii and are too small to be identified with a surfactant film. Further research and other experimental methods are required to elucidate both the physical meaning and the value of l with greater accuracy.

DISCUSSION AND CONCLUSION

The goal of this work was the systematic investigation of the size dependence of S_T under isothermal conditions. We avoided electrostatic contributions to the thermodiffusion behavior by using the nonionic surfactant $C_{12}E_5$ and performed measurements close to the *efb* to ensure spherical microemulsion droplets. In order to enable isothermal conditions, we varied the *n*-alkane from *n*-octane to *n*-tetradecane.

Because of the fact that the *efb* of the respective systems shifts to higher *n*-alkane concentrations with decreasing *n*-alkane chain length, the particle size can be increased while the temperature can be kept constant. This allows a systematic variation of the radius, keeping the chemistry of the microemulsion droplet interface the same. Neutron scattering experiments showed clearly that the radius of the droplets increases with decreasing *n*-alkane chain length and that the droplets have a spherical shape close to the *efb*. The Soret coefficient of the microemulsions with the different *n*-alkanes as a function of the radius can be described by a straight line, but with slightly larger deviations the data are also compatible with a quadratic dependence on the radius.

Furthermore, we studied the relation between the interfacial tension and the Soret coefficient (cf. eq 13). Assuming that the thickness of the transition layer l is temperature independent, l decreases from 6 to 1 Å by increasing the chain length of the *n*-alkane from 8 to 14. Considering that l is temperature dependent (cf. eq 14 and Figure 9), l lies between 1 and 2 Å and $(\partial l/\partial T)^{n\text{-alkane}}$ is on the order of a per mill relative to l decreasing with increasing chain length of the *n*-alkane. The decrease is reasonable because the size of the droplets also shrinks. Summarizing, we conclude that eq 13 is compatible with the thermodiffusion data of nonionic microemulsions and l is smaller than the diffuse amphiphilic film determined by SANS.

AUTHOR INFORMATION

Corresponding Authors

*T.S.: e-mail, thomas.sottmann@ipc.uni-stuttgart.de.
*S.W.: e-mail, s.wiegand@fz-juelich.de.

Notes

The authors declare no competing financial interest.

ACKNOWLEDGMENTS

The authors thank Reinhard Strey for his inspiring idea and Jan Dhont for his constant interest in this work and his support. Financial support from Deutsche Forschungsgemeinschaft Grants So 913 and Wi 1684 is gratefully acknowledged.

REFERENCES

(1) Weinert, F. M.; Mast, C. B.; Braun, D. Optical Fluid and Biomolecule Transport with Thermal Fields. *Phys. Chem. Chem. Phys.* **2011**, *13*, 9918−9928.

(2) Blanco, P.; Bou-Ali, M. M.; Platten, J. K.; Urteaga, P.; Madariaga, J. A.; Santamaria, C. Determination of Thermal Diffusion Coefficient in Equimolar *n*-Alkane Mixtures: Empirical Correlations. *J. Chem. Phys.* **2008**, *129*, 174504-1−174504-6.

(3) Ning, H.; Dhont, J. K. G.; Wiegand, S. Thermal-Diffusive Behavior of a Dilute Solution of Charged Colloids. *Langmuir* **2008**, *24*, 2426−2432.

(4) Wang, Z.; Kriegs, H.; Buitenhuis, J.; Dhont, J. K. G.; Wiegand, S. Thermophoresis of Charged Colloidal Rods. *Soft Matter* **2013**, *9*, 8697−8704.

(5) Piazza, R.; Parola, A. Thermophoresis in Colloidal Suspensions. *J. Phys.: Condens. Matter* **2008**, *20*, 153102−153120.

(6) Duhr, S.; Braun, D. Thermophoretic Depletion Follows Boltzmann Distribution. *Phys. Rev. Lett.* **2006**, *96*, 168301-1−168301-4.

(7) Vigolo, D.; Brambilla, G.; Piazza, R. Thermophoresis of Microemulsion Droplets: Size Dependence of the Soret Effect. *Phys. Rev. E* **2007**, *75*, R040401-1−R040401-4.

(8) Braibanti, M.; Vigolo, D.; Piazza, R. Does Thermophoretic Mobility Depend on Particle Size? *Phys. Rev. Lett.* **2008**, *100*, 108303-1−108303-4.
(9) Würger, A. Thermal Non-Equilibrium Transport in Colloids. *Rep. Prog. Phys.* **2010**, *73*, 126601−126636.
(10) Dhont, J. K. G.; Wiegand, S.; Duhr, S.; Braun, D. Thermodiffusion of Charged Colloids: Single-Particle Diffusion. *Langmuir* **2007**, *23*, 1674−1683.
(11) Naumann, P.; Becker, N.; Datta, S.; Sottmann, T.; Wiegand, S. Soret Coefficient in Nonionic Microemulsions: Concentration and Structure Dependence. *J. Chem. Phys. B* **2013**, *117*, 5614−5622.
(12) Strey, R. Microemulsion Microstructure and Interfacial Curvature. *Colloid Polym. Sci.* **1994**, *272*, 1005−1019.
(13) Kahlweit, M.; Strey, R.; Busse, G. Weakly to Strongly Structured Mixtures. *Phys. Rev. E* **1993**, *47*, 4197−4209.
(14) Menge, U.; Lang, P.; Findenegg, G. H.; Strunz, P. Structural Transition of Oil-Swollen Cylindrical Micelles of $C_{12}E_5$ in Water Studied by SANS. *J. Phys. Chem. B* **2003**, *107*, 1316−1320.
(15) Glatter, O.; Strey, R.; Schubert, K. V.; Kaler, E. W. Small Angle Scattering Applied to Microemulsions. *Ber. Bunsen-Ges. Phys. Chem. Chem. Phys.* **1996**, *100*, 323−335.
(16) Bernheim-Groswasser, A.; Tlusty, T.; Safran, S. A.; Talmon, Y. Direct Observation of Phase Separation in Microemulsion Networks. *Langmuir* **1999**, *15*, 5448−5453.
(17) Tlusty, T.; Safran, S. A.; Menes, R.; Strey, R. Scaling Laws for Microemulsions Governed by Spontaneous Curvature. *Phys. Rev. Lett.* **1997**, *78*, 2616−2619.
(18) Anderson, J. Colloid Transport by Interfacial Forces. *Annu. Rev. Fluid Mech.* **1989**, *21*, 61−99.
(19) Wiegand, S.; Ning, H.; Kriegs, H. Thermal Diffusion Forced Rayleigh Scattering Setup Optimized for Aqueous Mixtures. *J. Phys. Chem. B* **2007**, *111*, 14169−14174.
(20) Wang, Z.; Kriegs, H.; Wiegand, S. Thermal Diffusion of Nucleotides. *J. Phys. Chem. B* **2012**, *116*, 7463−7469.
(21) Wittko, G.; Köhler, W. Precise Determination of the Soret, Thermal Diffusion and Mass Diffusion Coefficients of Binary Mixtures of Dodecane, Isobutylbenzene and 1,2,3,4-Tetrahydronaphthalene by a Holographic Grating Technique. *Philos. Mag.* **2003**, *83*, 1973−1987.
(22) Kotlarchyk, M.; Chen, S. H. Analysis of Small-Angle Neutron-Scattering Spectra from Polydisperse Interacting Colloids. *J. Chem. Phys.* **1983**, *79*, 2461−2469.
(23) Foster, T.; Sottmann, T.; Schweins, R.; Strey, R. Small-Angle Neutron Scattering from Giant Water-in-Oil Microemulsion Droplets. I. Ternary System. *J. Chem. Phys.* **2008**, *128*, 54502.
(24) Rayleigh, L. The Incidence of Light upon a Transparent Sphere of Dimensions Comparable with the Wave-Length. *Proc. R. Soc. London, Ser. A* **1910**, *84*, 25−46.
(25) Gradzielski, M.; Langevin, D.; Magid, L.; Strey, R. Small-Angle Neutron-Scattering from Diffuse Interfaces. 2. Polydisperse Shells in Water−*n*-Alkane−$C_{10}E_4$ Microemulsions. *J. Phys. Chem.* **1995**, *99*, 13232−13238.
(26) Provencher, S. W. CONTIN: A General Purpose Constrained Regularization Program for Inverting Noisy Linear Algebraic and Integral Equations. *Comput. Phys. Commun.* **1982**, *27*, 229−242.
(27) Blanco, P.; Kriegs, H.; Lettinga, M. P.; Holmqvist, P.; Wiegand, S. Thermal Diffusion of a Stiff Rod-like Mutant Y21m-Fd-Virus. *Biomacromolecules* **2011**, *12*, 1602−1609.
(28) Burauer, S.; Sachert, T.; Sottmann, T.; Strey, R. On Microemulsion Phase Behavior and the Monomeric Solubility of Surfactant. *Phys. Chem. Chem. Phys.* **1999**, *1*, 4299−4306.
(29) Strey, R.; Winkler, J.; Magid, L. Small-Angle Neutron-Scattering from Diffuse Interfaces. 1. Monolayers and Bilayers in the Water Octane C12E5 System. *J. Phys. Chem.* **1991**, *95*, 7502−7507.
(30) Baxter, R. J. Percus−Yevick Equation for Hard Spheres with Surface Adhesion. *J. Chem. Phys.* **1968**, *49*, 2770−2774.
(31) Menon, S. V. G.; Manohar, C.; Rao, K. S. A New Interpretation of the Sticky Hard-Sphere Model. *J. Chem. Phys.* **1991**, *95*, 9186−9190.
(32) Foster, T.; Sottmann, T.; Schweins, R.; Strey, R. Small-Angle Neutron Scattering from Giant Water-in-Oil Microemulsion Droplets. I. Ternary System. *J. Chem. Phys.* **2008**, *128*, 054502-1−054502-13.
(33) Hellweg, T.; von Klitzing, R. Evidence for Polymer-like Structures in the Single Phase Region of a Dodecane/C12E5/Water Microemulsion: A Dynamic Light Scattering Study. *Physica A* **2000**, *283*, 349−358.
(34) Polyakov, P.; Luettmer-Strathmann, J.; Wiegand, S. Study of the Thermal Diffusion Behavior of Alkane/Benzene Mixtures by Thermal Diffusion Forced Rayleigh Scattering Experiments and Lattice Model Calculations. *J. Phys. Chem. B* **2006**, *110*, 26215−26224.
(35) Liu, G.; Giddings, J. C. Separation of Particles in Aqueous Suspensions by Thermal Field-Flow Fractionation. Measurement of Thermal-Diffusion Coefficients. *Chromatographia* **1992**, *34*, 483−492.
(36) Parola, A.; Piazza, R. Particle Thermophoresis in Liquids. *Eur. Phys. J. E* **2004**, *15*, 255−263.
(37) Sottmann, T.; Strey, R. Ultralow Interfacial Tensions in Water-*n*-Alkane-Surfactant Systems. *J. Chem. Phys.* **1997**, *106*, 8606−8615.
(38) Vonnegut, B. Rotating Bubble Method for the Determination of Surface and Interfacial Tensions. *Rev. Sci. Instrum.* **1942**, *13*, 6−9.
(39) Sottmann, T.; Strey, R. Shape Similarities of Ultra-Low Interfacial Tension Curves in Ternary Microemulsion Systems of the Water-Alkane-C(i)E(j) Type. *Ber. Bunsen-Ges. Phys. Chem.* **1996**, *100*, 237−241.
(40) Kahlweit, M.; Strey, R.; Busse, G. Microemulsions: A Qualitative Thermodynamic Approach. *J. Phys. Chem.* **1990**, *94*, 3881−3894.
(41) Leitao, H.; Somoza, A. M.; daGama, M. M. T.; Sottmann, T.; Strey, R. Scaling of the Interfacial Tension of Microemulsions: A Phenomenological Description. *J. Chem. Phys.* **1996**, *105*, 2875−2883.